Clim. Past Discuss., 10, 2519–2546, 2014
www.clim-past-discuss.net/10/2519/2014/
doi:10.5194/cpd-10-2519-2014

Climate of the Past Discussions
Open Access

An abrupt slowdown of Atlantic Meridional Overturning Circulation during 1915–1935 induced by solar forcing in a coupled GCM

P. Lin[1], Y. Song[1,2], Y. Yu[1], and H. Liu[1]

[1]State Key Laboratory of Numerical Modeling for Atmospheric Sciences and Geophysical Fluid Dynamics (LASG), Institute of Atmospheric Physics (IAP), Chinese Academy of Sciences, Beijing 100029, China
[2]College of Earth Science, University of Chinese Academy of Sciences, Beijing 100049, China

Received: 9 May 2014 – Accepted: 2 June 2014 – Published: 18 June 2014

Correspondence to: Y. Song (songy@mail.iap.ac.cn)

Published by Copernicus Publications on behalf of the European Geosciences Union.

Abstract

In this study, we explore an abrupt change of Atlantic Meridional Overturning Circulation (AMOC) apparent in the historical run simulated by the second version of the Flexible Global Ocean–Atmosphere–Land System model – Spectral Version 2 (FGOALS-s2). The abrupt change is noted during the period from 1915 to 1935, in which the maximal AMOC value is weakened beyond 6 Sv (1 Sv = 10^6 m^3 s^{-1}). The abrupt signal first occurs at high latitudes (north of 46° N), then shifts gradually to middle latitudes (~ 35° N) three to seven years later. The weakened AMOC can be explained in the following. The weak total solar irradiance (TIS) during early twentieth century decreases pole-to-equator temperature gradient in the upper stratosphere. The North polar vortex is weakened, which forces a negative North Atlantic Oscillation (NAO) phase during 1905–1914. The negative phase of NAO induces anomalous easterly winds in 50–70° N belts, which decrease the release of heat fluxes from ocean to atmosphere and induce surface warming over these regions. Through the surface ice–albedo feedback, the warming may lead to continuously melting sea ice in Baffin Bay and Davis Strait, which results in freshwater accumulation. This can lead to salinity and density reductions and then an abrupt slowdown of AMOC. Moreover, due to increased TIS after 1914, the enhanced Atlantic northward ocean heat transport from low to high latitudes induces an abrupt warming of sea surface temperature or upper ocean temperature in mid–high latitudes, which can also weaken the AMOC. The abrupt change of AMOC also appears in the PiControl run, which is associated with the lasting negative NAO phases due to natural variability.

1 Introduction

The Atlantic meridional overturning circulation (AMOC) is a major thermohaline circulation characterized by a northward flow of warm, salty water in the upper Western Atlantic Ocean and a southward flow of colder water in the deep Atlantic (Kuhlbrodt

CPD
10, 2519–2546, 2014

et al., 2007). Changes in the AMOC can impact greatly the North American and European climate (Rahmstorf, 2003; Sutton and Hodson, 2005), Atlantic Multi-decadal Oscillation (Latif et al., 2004; Zhang et al., 2007), variability of Arctic sea ice (Mahajan et al., 2011), the intertropical convergence zone (Vellinga and Wood, 2002; Cheng et al., 2007; Chiang et al., 2008) and El Niño–Southern Oscillation (Timmermann et al., 2005, 2007).

The abrupt slowdown of AMOC had been found in the paleoclimatic proxy records (Broecker et al., 1985; Sarnthein et al., 1994; Clark et al., 2002). Such changes had been linked to freshwater discharge into the North Atlantic from the melting ice sheets (McManus et al., 2004; Clark et al., 2001, 2002). Numerical simulations suggested that increased greenhouse gas concentrations may lead to a significant weakening or even a collapse of AMOC (Manabe and Stouffer, 1993; Stocker and Schmittner, 1997; Wood et al., 1999; Gregory et al., 2005). By increasing freshwater inputs (waterhosing experiments) in the northern high-latitude Atlantic in the numerical models, an abrupt slowdown of AMOC had also occurred due to weakened convection caused by less-dense seawater (Vellinga and Wood, 2002; Levermann et al., 2005; Zhang and Delworth, 2005; Timmermann et al., 2005, 2007). However, driven by realistic external forcing, no studies show climate models with coarse resolution have the abilities to simulate the abrupt change of AMOC. Whether the climate model can simulate the abrupt change of AMOC? What process causes the abrupt change? What is the difference between the abrupt change driven by realistic forcing and have been occurred in the proxy records?

The rest of the paper is organized in the following manner. In Sect. 2, we describe the coupled model FGOALS-s2, experiments and data used for analysis. The appearance and attribution of an abrupt slowdown of AMOC in historical simulations is described in Sect. 3. Discussions and conclusions are presented in Sect. 4.

CPD
10, 2519–2546, 2014

2 Model, data and method

The second version of the Flexible Global Ocean–Atmosphere–Land System model–Spectral Version 2 (FGOALS-s2) is one of the members in the Coupled Model Intercomparison Project Phase 5 (CMIP5, Taylor et al., 2012). FGOALS includes atmospheric, oceanic, sea ice, land, and the coupler components, which have been reported by Bao et al. (2013) and Lin et al. (2013). The historical simulations used here have been integrated over the period 1850–2005 and forced by observed natural and anthropogenic forcings, which are designed as CMIP5 historical experiments. Three historical runs had been done in FGOALS-s2. The changes of AMOC during 1915–1935 are similar but the magnitude of AMOC change slightly weaker in the two historical runs. Thus, we choose only one historical run with the most significantly abrupt change of AMOC to do the following analysis.

In this study, we use the moving t test technique (MTT, Jiang and You, 1996) to detect the time of abrupt change by identifying whether the significant difference exists in the mean values of two subsamples in a time series. To do this, two subsamples (y_1 and y_2 with equivalent time lengths) are chosen before and after the change point.

The t statistic is calculated as follows:

$$t = \frac{\overline{y_2} - \overline{y_1}}{s\sqrt{\frac{1}{n_1} + \frac{1}{n_2}}}, \quad (1)$$

where $s = \sqrt{\frac{n_1 s_1^2 + n_2 s_2^2}{n_1 + n_2 - 2}}$, n_i, $\overline{y_i}$, s_i^2 ($i = 1, 2$) denote the time lengths, the mean values and the variances for the two subsamples, respectively. For a significance level α, the time of abrupt change is corresponding to the wave crests or troughs of the periods ($|t| \geq t_\alpha$).

CPD
10, 2519–2546, 2014

3 Results

3.1 An abrupt slowdown of AMOC

Figure 1a shows the time series of the maximal AMOC at three different latitudes in the historical run of FGOALS-s2. The simulated maximal AMOC at 26.5° N is approximately 21.1 ± 2.7 Sv (1 Sv = 10^6 m^3 s^{-1}), which is slightly larger than the observed value (18.7 ± 5.6 Sv) at this latitude (Cunningham et al., 2007). During the period 1915–1935 at latitude 26.5° N, a remarkably abrupt slowdown (~ 6 Sv) is apparent (Fig. 1a). The corresponding abrupt year is approximately 1928 at this latitude. The AMOC reaches its peak of approximately 24 Sv in 1920 and weakens to approximately 18 Sv in 1935. At latitudes 36° N and 60° N, the abrupt changes appear earlier than those at latitude 26.5° N. The abrupt changes at 60° N and 36° N lead that at 26.5° N approximately seven years (1921) and three years (1925) earlier, respectively, with corresponding significant linear correlation coefficients of 0.51 and 0.8, respectively. This indicates the abrupt change of the AMOC occurred at high latitudes then extending to middle latitudes. Approximately two to three decades after the abrupt change, the AMOCs are restored to magnitudes with values approximately 1–2 Sv smaller than those before the abrupt change.

The abrupt changes of AMOC can also be found in other two historical runs by FGOALS-s2 (Fig. S1a and b in the Supplement). The magnitudes and times of abrupt change in other two historical runs are slightly different from that in the used historical run. In these historical runs, all the abrupt changes appear first at the high latitude and then at the middle latitude. In the PiControl run, the abrupt-like change of AMOC is also found, for instance, abrupt slowdown appears during 180–240 with the value of 3–4 Sv (Fig. S1c in the Supplement). Such kind of abrupt change begins at the high latitude and moves to the middle high latitude as that in the historical runs. The related reason will be discussed in the following.

Spatially, the maximal AMOC is located near latitudes 30° N and 36° N and at a depth of 1200 m with a value of approximately 21 Sv (Fig. 1b). The change is significant in

CPD
10, 2519–2546, 2014

the entire depth, particularly from 30° S to 60° N (Fig. 1b). After the abrupt change, the maximal magnitude (~ 6 Sv, > 30 % of the total magnitude) of the weakened AMOC is located between 30° N and 40° N at a depth of 2000–3000 m (Fig. 1b). MTT was used to determine that the abrupt change occurred initially during 1920–1921, as shown in Fig. 1a, at high latitudes of 46–60° N (Fig. 1c). The signal of abrupt change persists from 200 m to 3500 m and appears again between 1922 and 1924 at 42–46° N and between 1925 and 1927 at 34–42° N. At 26.5° N, an abrupt change is also noted in 1928 below 1000 m. This analysis indicates an abrupt slowdown (~ 6 Sv) of AMOC during 1915–1935 that occurred first at high latitudes (> 46° N) and then at low–middle latitudes (Fig. 1). Next, we will investigate the reasons for the abrupt change of AMOC during 1915–1935.

3.2 Reasons for the abrupt slowdown

The formation of North Atlantic Deep Water (NADW) or AMOC is closely connected to deep convection (DC), the sites of which can be identified by mixed-layer depth (MLD). In FGOALS-s2, the main sites of DC (indicated by deep MLD) are located in the Labrador Sea east of Greenland and south of Iceland in the North Atlantic (Fig. 2a). The simulated sites of DC are comparable with the observation (Marshall and Schott, 1999; Curry et al., 1999). The differences (Fig. 2b) in MLD between the periods of 1920–1930 and 1910–1920 show that after the abrupt change, the MLD became shallow (> 200 m), almost following the locations of deepest MLD. The most obvious change in MLD (> 800 m) is tilting to the northwest in the Labrador Sea between 50° N and 65° N, which indicates a reduction in DC. To determine whether the DC caused the abrupt change of the AMOC, the years of abrupt change in MLD were identified (Fig. 2c). Earlier abrupt changes appeared in 1917 near the Davis Strait and near the location (55° N, 38° W) south of Greenland. Such abrupt MLD signals occurred earlier in these areas than in those at north of 45° N and south of 65° N (Fig. 2c). Such changed signals may be important sources for the cause of the abrupt slowdown of AMOC. North of Iceland, abrupt changes in MLD signals also appear earlier than those of AMOC. Although the

CPD
10, 2519–2546, 2014

abrupt change in MLD occurred during 1916–1918 near the Mediterranean, the MLDs are shallower than 200 m in these regions. Thus, we next focus on investigating the abrupt changes in DC regions, particularly in the two boxes (box A: 60–45° W, 50–65° N; box B: 40–30° W, 50–60° N).

Density anomalies can result in DC changes. In this section, we identify whether temperature and salinity anomalies contributed to density anomalies shown in the two boxes in Fig. 3. For box A (60–45° W, 50–65° N), beginning in 1916 or 1917, a remarkably abrupt change is noted in surface density and salinity, with continued weakening until 1927 (Fig. 3a). Furthermore, in 1900–1917 and 1917–1950, the correlation coefficients between surface density and salinity are significantly high (> 0.7, with 95 % confidence, Table 1). Moreover, high correlations also appear for averaged upper–300 m density and salinity. However, temperature variations exhibit relatively moderate changes during 1915–1930 (Fig. 3a). Although a high negative correlation appears before 1917, a weak correlation is noted after 1917 for that between density and temperature, and no significant correlation exists between density and temperature in the upper 300 m range. These findings indicate that the contribution of salinity is important for density at the surface and at deep layers in box A. For temperature, surface change may be more important than that at the deep layer. Given the contributions of salinity and temperature, the abrupt density change in 1917 in box A is mainly contributed by salinity. The fresher seawater led to light density, causing shallow MLD or weakened DC in this region.

For box B (40–30° W, 50–60° N), as shown in Fig. 3b, regional averaged density also experienced an abrupt decrease in approximately 1917 that lasted until 1927. In contrast to that in box A, more consistent changes are present between the density and the temperature in box B, with significant negative correlations of −0.83 and −0.92 occurring before and after 1917, respectively (Table 1). After 1917, however, the correlation between density and salinity is very weak, even exhibiting a negative value. These findings indicate the contribution of temperature anomalies to density in box B were more

CPD
10, 2519–2546, 2014

important than that of salinity during the abrupt processes. Thus, the warmer seawater anomaly shown in box B led to light density, causing shallow MLD or reductive DC.

In this analysis, we have shown that in box A, surface or upper salinity changes were responsible for the changes in surface or upper density. To identify whether the salinity anomalies in box A were caused by the melting of sea ice at high latitudes, particularly in Davis Strait and Baffin Bay, the differences between mean sea ice concentration averaged from 1913 to 1920 and sea ice concentration averaged from 1900 to 1912 from April to September are displayed in Fig. 4a. The most obvious differences are focused on the interface of Baffin Bay and Davis Strait and at the exit of Hudson Bay. Along Greenland's western coast, the most significant reduction of sea ice concentration is approximately 20 %, corresponding to a reduction in sea ice cover of 8×10^2 km^2. However, in box A, as shown in Fig. 4a, the sea ice concentration averaged from 1900 to 1912 and from April to September is almost zero. This reduction in salinity in box A may be caused by the increased freshwater transport from high latitudes such as from Baffin Bay and Davis Strait. Furthermore, the time series of regional (60–70° N, 65–50° W) integral sea ice cover averaged from April to September also shows characteristics of sea ice reduction in 1913–1920 (Fig. 3c, black line). Since 1913, the obviously negative anomalies of sea ice cover have appeared with a reduction of approximately 0.35×10^5 km^2 relative to the sea ice cover averaged from 1850 to 1912 that lasted for seven years (1913–1920) with a minimal value in 1915.

The differences between sea surface temperatures (SSTs) averaged from 1913 to 1920 and that averaged from 1900 to 1912 from April to September are displayed in Fig. 4b. The largest positive differences (~ 1 K) are focused on the interface of Baffin Bay and Davis Strait, and a positive anomaly is noted east of Labrador Sea, which may have caused the changes of density in this region (Fig. 4b). The time series of regional (60–70° N, 65–50° W) averaged SST shows a significant warming since 1913 that lasted seven years until 1920 (Fig. 3c, red line), which relates to a reduction in sea ice cover with a high negative correlation of −0.54 from 1890 to 1950. Amplified by the ice–albedo feedback in a warming state (Fig. 3c, red line), reductions in sea ice cover

CPD
10, 2519–2546, 2014

(same as 1913 in Fig. 3c, black line) will expose the dark underlying ocean, allowing more solar radiation to be absorbed (Fig. 3c, blue line, with a high negative correlation of −0.72 with sea ice cover), which enhances warming and leads to further ice melting. Previous studies that use climate models also indicate a polar amplification of greenhouse gas-induced warming via positive feedback between air temperature, ice extent, and surface albedo (Manabe et al., 1991; Murphy and Mitchell, 1995). Therefore, we suggest that because of the positive feedback, a small reduction in sea ice cover or local surface temperature warming may have been amplified to result in an abrupt slowdown of AMOC in later years.

In box B (40–30° W, 50–60° N), the warming is responsible for the abrupt reduction in surface or upper density (Fig. 3b). Significant warming anomalies are noted between 45–60° N with a maximal warming magnitude of approximately 1 K (SST difference, 1917–1918 minus 1910–1916, Fig. 4c). Warming also appears on the east coast near the Mediterranean. To identify the reasons for the significant SST warming shown in box B, the northward ocean heat transport (OHT) in the Atlantic is presented in Fig. 4d. Significant positive anomalies appear from 1916 to 1927 over the North Atlantic. The most obvious OHT appears first from 30° N to 40° N in approximately 1917 and extends to 60° N in approximately 1921. Because the northward OHT increases from low to high latitudes, the SST or upper sea temperature, in these regions exhibits an abrupt warming that persisted for several years (Figs. 3b and 4c). The warming in the region leads to the decreased density, which induces the slowdown of AMOC. Previous studies have reported that the northward OHT can cause sea temperature change in the North Atlantic (Broecker et al., 1985; Crowley, 1992). Moreover, the net surface heat flux anomalies are also examined (not shown here). The positive SST anomalies correspond to negative net surface heat fluxes since 1917, which implies that the heat fluxes limited the warming in this region. Therefore, it can be concluded that in box B, the enhanced northward OHT contributes to surface or upper warming, which decreases the seawater density in the upper layer. This density reduction stabilizes the water column, inhibites DC formation, and ultimately leads to the slowdown of AMOC.

CPD
10, 2519–2546, 2014

3.3 The forcing of solar irradiances

As mentioned above, the abrupt slowdown of AMOC is the combined results of enhanced northward OHT from low to high latitudes and the melting sea ice or warming surface temperature in high latitudes. We will reveal which process results in these changes in the next. Time evolution of the total solar irradiance (TSI) used in CMIP5 historical simulations (Fig. 5a) shows that there is a very weak peak during 1905–1909 compared with other previous peaks from 1860 to 1895 and the following peaks after 1914. Combined with the following crest, the TSI is abnormally low from 1900 to 1914. After 1914, the TIS experiences the significant increases with a peak in 1918. The value with the peak in 1918 is larger than that in 1905 and in 1895. The meridional TIS difference (1916–1924 minus 1860–1900) shows the obvious increases over tropics, with the value of incoming shortwave radiation at the top-of-atmosphere (TOA) about 0.036 $W\,m^{-2}$ (Fig. 5b). The increased radiation value can warm the SST over the tropics, and enhance northward OHT from low to high latitudes, which warms the high-latitude SST and finally slows down the AMOC (as mentioned in Sect. 3.2).

Another aspect, under the forcing of the weak TIS from 1900 to 1914, there is a decrease in temperature in the upper stratosphere (Fig. 6). This temperature decrease is directly attributable to the decrease in ozone heating associated with solar ultraviolet irradiance (Fig. 5a, Haigh et al., 2010). This signal reaches its peaks in the tropics and decreases as it goes poleward, which produces a relative decrease in the pole-to-equator temperature gradient. As shown in Fig. 6, both weak peak (1905–1908) and following crest (1911–1914) show the obvious cooling near the mid–low latitude upper stratosphere. In 1906, the maximal cooling can reach about 2 K (Fig. 6b). This weakened poleward temperature gradient will cause a weak easterly wind anomaly in the mid-latitude zonal mean circulation in the upper stratosphere according to geostrophic balance. This anomaly then propagates poleward and downward and amplifies as it does so, producing a weaker polar vortex (Kodera, 1995; Kodera and Kuroda, 2002). This process is well reproduced in the coupled model. In 1905, the easterly (i.e., neg-

CPD
10, 2519–2546, 2014

ative between 40–60° N) anomalies of 4 m s^{-1} are found (Fig. 7a) and move poleward and downward from 1906 to 1908 (Fig. 7b–d), while positive zonal wind anomalies are found at mid–low latitudes (Fig. 7a–d). Analogously, in 1911, weak easterly anomalies of 1 m s^{-1} are seen south of 60° N and then move poleward and downward from 1912 to 1914 with the maximal amplitude of 4–5 m s^{-1} around 50° N, whereas positive anomalies are also found at mid–low latitudes (Fig. 7e–7h). These zonal wind dipole anomalies are located in the lower stratosphere and the whole troposphere during these two periods. Propagation and amplification of this kind of zonal wind dipole anomaly are associated with planetary-scale Rossby wave activity (Hines, 1974; Kuroda and Kodera, 2002). Many studies have pointed out the zonal wind dipole anomalies in the troposphere and Earth surface can produce an anomalously negative phase of North Atlantic Oscillation (NAO) (e.g., Kodera, 2002; Tourpali et al., 2003; Baldwin and Dunkerton, 2005). As shown in Fig. 8, the NAO phase (negative index) is negative from 1905 to 1914 with the weak strength of Icelandic low and Azores high. As a response to the negative phase of NAO, in the subpolar regions, the cyclone circulation weakens, and anomalous easterly wind reduces the cold air transport in the high latitude. These decrease air–sea temperature differences in the belts between 50–70° N and then reduce heat release from the ocean to the atmosphere by reducing sensible and latent heat fluxes, and lead to warming over these regions. Through surface ice–albedo feedback, a local surface temperature warming may induce the significant reduction of sea ice cover in Baffin Bay and Davis Strait (Figs. 3c and 4a), and finally lead to an abrupt slowdown of AMOC in later years (as mentioned in Sect. 3.2).

4 Summary and discussions

In this study, we find an abrupt slowdown of AMOC during 1915–1935 in the historical runs simulated by FGOALS-s2. The abrupt slowdown can be attributable to the change of solar radiation. The weak TIS from 1900 to 1914 induces negative temperature anomalies near the mid–low latitude upper stratosphere and results in a relative

CPD
10, 2519–2546, 2014

decrease in the pole-to-equator temperature gradient. As a response to the diminished poleward temperature gradient, a weak easterly wind anomaly in the mid-latitude zonal mean circulation appears in the upper stratosphere, then propagates poleward and downward over the lower stratosphere and the whole troposphere. These anomalies can produce an anomalous negative NAO pattern during 1905–1914. The negative phase of NAO induces anomalous easterly wind in belts of 50–70° N, which decreases heat release from ocean to atmosphere, and leads to surface warming over these regions. Through the surface ice–albedo feedback, the surface warming may lead to continuously melting sea ice in Baffin Bay and Davis Strait, which results in freshwater accumulation. After seven years, the buildup of freshwater may cause a serious reduction of surface and upper-ocean salinity, thereby reducing the density in the Labrador Sea, which increases its stability and inhibits DC formation. Moreover, after 1914, the TIS experiences the significant increases with a peak in 1918 and the large increases over tropics, which warms the SST over the tropics, and enhances northward OHT from low to high latitudes. These can also induce a warming of SST or upper ocean temperature in mid–high latitudes. The warming leads to a reduction in density, which can stabilize the water column, inhibit the formation of DC, and finally lead to the slowdown of AMOC.

In other two historical runs, the abrupt changes also appear during 1915–1935 (Fig. S1a and b in the Supplement). There are still weakened pole-to-equator temperature gradients, zonal wind anomalies (no shown) and negative NAO phases before the abrupt change of AMOC although the magnitudes of AMOC abrupt change are different (Fig. S2a and b in the Supplement). Meanwhile, there is enhanced northward OHT in the North Atlantic (Fig. S3a and b in the Supplement). Such similar processes indicate the change in solar radiation (from extremely low to high) plays an important role in the abrupt change during 1915–1935. In the PiControl run, there are also the abrupt changes, such as changes during 180–200. Before the abrupt change, the negative NAO phases occur during 177–181 (Fig. S2c in the Supplement). This will induce an accumulating melting of sea ice. The melting causes the freshwater input into the

CPD
10, 2519–2546, 2014

North Atlantic Ocean and then light density. The light density can lead to the weakened convective and the abrupt change of AMOC. In the PiControl run, before the abrupt change, the enhanced northward OHT in the Atlantic cannot be found (Fig. S3c in the Supplement), which is different from that in the historical runs. Thus, the lasting negative NAO phases may lead to the abrupt changes of AMOC in the PiControl runs, in which the TSI is fixed at the preindustrial level. These indicate that the abrupt change in the PiControl run may be a result of natural variability. However, in three historical runs, solar radiation (from extremely low to high) is responsible for the abrupt change during 1915–1935.

Our study shows that in the historical runs in FGOALS-s2, the weakened AMOC is found around 1920. Does any observational evidence support the simulated weakened AMOC during 1915–1935? According to different reconstruction data, around 1920, the weakened AMOC had been found (Latif et al., 2004; Knight et al., 2005; Cheng et al., 2009). Interestingly, the abrupt-like change of AMOC was presented during 1910–1930 in Latif et al. (2004). This suggests the AMOC can present a decadal change or abrupt change during 1910–1930, which supports the simulation result in present study.

Felis et al. (2009) found an abrupt freshening appeared during 1905–1910 in the western subtropical North Pacific. The abrupt change was associated with weak Kuroshio transport driven by weak westerlies and southwesterlies. They argued the abrupt event in the western North Pacific preceded that in the North Atlantic by a few years. In the historical simulation by FGOALS-s2, an obvious freshening appears during 1905–1912 from the sea surface salinity (SSS, Fig. S4 in the Supplement). The freshening comes back to normal value after 1925, which is different from the continually low level of SSS in their study (Felis et al., 2009). The simulated SLP differences between 1910–1920 and 1900–1905 present an anomalous high SLP over northeast Asia and low SLP over the western subtropical North Pacific (Fig. S5 in the Supplement). These features had been pointed out by Felis et al. (2009). Furthermore, the winter SLP from the northeast Asian atmospheric anomaly center shows a significant increasing from 1900 to 1916 (Fig. S4 in the Supplement). Based on the detail explana-

CPD
10, 2519–2546, 2014

tions in Felis et al. (2009), these atmospheric anomalies can result in the freshening of SSS over the western subtropical North Pacific. Meanwhile, as shown in Fig. S5 in the Supplement, the SLP spatial differences in the North Hemisphere may correspond to the negative phase of Arctic Oscillation (AO). Thus, it is very likely that the freshening in western subtropical North Pacific may also a result of solar irradiance in the early twentieth century. The obvious freshening of SSS, increased high SLP over northeast Asia and negative AO phase can partly support the possible abrupt change of AMOC in the North Atlantic, which is induced by the changes of TIS during early twentieth century.

Do other models also simulate the weakened AMOC around 1920? According to SODA reanalysis, the AMOC also weakened around 1920 (Schott et al., 2009). In the meanwhile, some models in CMIP5 also simulated a declining AMOC around 1920 (Menary et al., 2013; Menary and Scaife, 2014). In the present study the AMOC experiences the significantly abrupt slowdown. Different from the study, Menary and Scaife (2014) argued the weakened AMOC around 1920 was a part of multidecadal variability. These differences may be associated with inter-model differences in response to the solar forcing. Thus, it is necessary to examine whether most of models can simulate the weakening or abrupt change of AMOC around 1920. Given that only one single coupled model is used in this study, this may result in model-dependent conclusions. Therefore, it is very necessary to use multi-model simulations to validate these conclusions.

Driven by realistic forcing, the abrupt change lasts about 20–30 years during 1910s–1930s in FGOALS-s2. The time length is similar to that derived from waterhosing experiments (Zhang and Delworth, 2005; Timmermann et al., 2005, 2007). However, the experienced time length is shorter than century time length in paleoclimatic proxy records (Sarnthein et al., 1994; Clark et al., 2002) or in the simulation using unchanged external forcing (Hall and Stouffer, 2001; Goosse et al., 2002; Drijfhout et al., 2013). These results almost involve the melting of sea ice or the caused freshwater inputting into the convection zones, which will shut down the deep convection and induce the

CPD
10, 2519–2546, 2014

abrupt change of AMOC. In the study, another important process to affect the AMOC change is the enhanced OHT from low to high latitude. Combined with the melting of sea ice, the enhanced OHT that induced by the changes of TIS may enhance the abrupt changes of AMOC. This conclusion needs to be detected in other CMIP5 coupled models. Meanwhile, the abrupt change of AMOC can reach 6 Sv in the historical run used for detailed analysis. For the other two historical runs, the maximal magnitudes are about 5 Sv and 4.5 Sv, respectively. The magnitudes are slightly larger than that in the PiControl run (about 4 Sv), which may be associated with the change of TSI. In the present study, the significant AMOC changes may be due to high climate sensitivity in FGOALS-s2 (Chen et al., 2014).

The Supplement related to this article is available online at doi:10.5194/cpd-10-2519-2014-supplement.

Acknowledgements. We acknowledge Aixue Hu for his comments and suggestions. This project is supported by the National Key Program for Developing Basic Sciences (Grant No. 2010CB950502), the National Natural Science Foundation of China (Grant Nos. 41376019 and 41023002).

References

Baldwin, M. P. and Dunkerton, T. J.: The solar cycle and stratosphere–troposphere dynamical coupling, J. Atmos. Sol.-Terr. Phy., 67, 71–82, 2005.

Bao, Q., Lin, P., Zhou, T. et al.: The flexible global ocean–atmosphere–land system model, spectral version 2: FGOALS-s2, Adv. Atmos. Sci., 30, 561–576, 2013.

Broecker, W. S., Peteet, D. M., and Rind, D.: Does the ocean–atmosphere system have more than one stable mode of operation?, Nature, 315, 21–26, 1985.

Chen, X. L., Zhou, T. J., and Guo, Z.: Climate sensitivities of two versions of FGOALS model to idealized radiative forcing, Science China Earth Sciences, 57, 1363–1373, doi:10.1007/s11430-013-4692-4, 2014.

CPD
10, 2519–2546, 2014

Cheng, J., Guo, P., Zhang, F., Liu, Z., Liu, L., and Qiu, W.: Reconstructing changes in Atlantic thermohaline circulation during the 20th century under two possible scenarios, Science China Earth Sciences, 56, 258–269, doi:10.1007/s11430-012-4465-5, 2013.

Cheng, W., Bitz, C. M., and Chiang, J. C. H.: Adjustment of the global climate to an abrupt slowdown of the Atlantic meridional overturning circulation, Geoph. Monog. Series, 173, 295–313, 2007.

Chiang, J. C. H., Cheng, W., and Bitz, C. M.: Fast teleconnections to the tropical Atlantic sector from Atlantic thermohaline adjustment, Geophys. Res. Lett., 35, L07704, doi:10.1029/2008GL033292, 2008.

Clark, P. U., Marshall, S. J., Clarke, G. K. C. et al.: Freshwater forcing of abrupt climate change during the last glaciations, Science, 293, 283–287, 2001.

Clark, P. U., Pisias, N. G., Stocker, T. F. et al.: The role of the thermohaline circulation in abrupt climate change, Nature, 415, 863–869, 2002.

Crowley, T. J.: North Atlantic deep water cools the Southern Hemisphere, Paleoceanography, 7, 489–497, 1992.

Cunningham, S. A., Kanzow, T., Rayner, D. et al.: Temporal variability of the Atlantic meridional overturning circulation at 26.5° N, Science, 317, 935–938, 2007.

Curry, W. B., Marchitto, T. M., McManus, J. F. et al.: Millennial-scale changes in ventilation of the thermocline, intermediate, and deep waters of the glacial North Atlantic, in: Mechanisms of Global Climate Change at Millennial Time Scales, 59–76, 1999.

Drijfhout, S., Gleeson, E., Dijkstra, H. A. et al.: Spontaneous abrupt climate change due to an atmospheric blocking–sea-ice–ocean feedback in an unforced climate model simulation, P. Natl. Acad. Sci. USA, 110, 19713–19718, 2013.

Felis, T., Suzuki, A., Kuhnert, H. et al.: Subtropical coral reveals abrupt early-twentieth-century freshening in the western North Pacific Ocean, Geology, 37, 527–530, 2009.

Goosse, H., Renssen, H., Selten, F. M., Haarsma, R. J., and Opsteegh, J. D.: Potential causes of abrupt climate events: a numerical study with a three-dimensional climate model, Geophys. Res. Lett., 29, 7-1–7-4, 2002.

Gregory, J. M., Dixon, K. W., Stouffer, R. J. et al.: A model intercomparison of changes in the Atlantic thermohaline circulation in response to increasing atmospheric CO_2 concentration, Geophys. Res. Lett., 32, , L12703, doi:10.1029/2005GL023209, 2005.

Haigh, J. D., Winning, A. R., Toumi, R. et al.: An influence of solar spectral variations on radiative forcing of climate, Nature, 467, 696–699, 2010.

CPD
10, 2519–2546, 2014

Hall, A. and Stouffer, R. J.: An abrupt climate event in a coupled ocean–atmosphere simulation without external forcing, Nature, 409, 171–174, 2001.
Hines, C. O.: A possible mechanism for the production of sun-weather correlations, J. Atmos. Sci., 31, 589–591, 1974.
Knight, J. R., Allan, R. J., Folland, C. K., Vellinga, M., and Mann, M. E.: A signature of persistent natural thermohaline circulation cycles in observed climate, Geophys. Res. Lett., 32, L20708, doi:10.1029/2005GL024233, 2005.
Kodera, K.: On the origin and nature of the interannual variability of the winter stratospheric circulation in the Northern Hemisphere, J. Geophys. Res.-Atmos., 100, 14077–14087, 1995.
Kodera, K.: Solar cycle modulation of the North Atlantic Oscillation: implication in the spatial structure of the NAO, Geophys. Res. Lett., 29, 8, doi:10.1029/2001GL014557, 2002.
Kodera, K. and Kuroda, Y.: Dynamical response to the solar cycle, J. Geophys. Res., 107, 4749, 2002.
Kuhlbrodt, T., Griesel, A., Montoya et al.: On the driving processes of the Atlantic meridional overturning circulation, Rev. Geophys., 45, RG2001, doi:10.1029/2004RG000166, 2007.
Latif, M., Roeckner, E., Botzet, M. et al.: Reconstructing, monitoring, and predicting multidecadal-scale changes in the North Atlantic thermohaline circulation with sea surface temperature, J. Climate, 17, 1605–1614, 2004.
Levermann, A., Griesel, A., Hofmann, M. et al.: Dynamic sea level changes following changes in the thermohaline circulation, Clim. Dynam., 24, 347–354, 2005.
Lin, P., Yu, Y., and Liu, H.: Long-term stability and oceanic mean state simulated by the coupled model FGOALS-s2, Adv. Atmos. Sci., 30, 175–192, 2013.
Mahajan, S., Zhang, R., and Delworth, T. L.: Impact of the Atlantic Meridional Overturning Circulation (AMOC) on Arctic surface air temperature and sea ice variability, J. Climate, 24, 6573–6581, 2011.
Manabe, S. and Stouffer, R. J.: Century-scale effects of increased atmospheric CO_2 on the ocean–atmosphere system, Nature, 364, 215–218, 1993.
Manabe, S., Stouffer, R. J., Spelman, M. J. et al.: Transient responses of a coupled ocean–atmosphere model to gradual changes of atmospheric CO_2. Part I. Annual mean response, J. Climate, 4, 785–818, 1991.
Marshall, J. and Schott, F.: Open-ocean convection: observations, theory, and models, Rev. Geophys., 37, 1–64, 1999.

CPD
10, 2519–2546, 2014

McManus, J. F., Francois, R., Gherardi, J. M. et al.: Collapse and rapid resumption of Atlantic meridional circulation linked to deglacial climate changes, Nature, 428, 834–837, 2004.
Menary, M. B. and Scaife, A. A.: Naturally forced multidecadal variability of the Atlantic meridional overturning circulation, Clim. Dynam., 42, 1347–1362, 2014.
Menary, M. B., Roberts, C. D., Palmer, M. D. et al.: Mechanisms of aerosol-forced AMOC variability in a state of the art climate model, J. Geophys. Res.-Oceans, 118, 2087–2096, 2013.
Murphy, J. M. and Mitchell, J. F. B.: Transient response of the Hadley Centre coupled ocean–atmosphere model to increasing carbon dioxide. Part II: Spatial and temporal structure of response, J. Climate., 8, 57–80, 1995.
Rahmstorf, S.: Thermohaline circulation: the current climate, Nature, 421, 699, doi:doi:10.1038/421699a, 2003.
Sarnthein, M., Winn, K., Jung, S. J. A. et al.: Changes in east Atlantic deepwater circulation over the last 30,000 years: eight time slice reconstructions, Paleoceanography, 9, 209–267, 1994.
Schott, F. A., Stramma, L., Giese, B. S. et al.: Labrador Sea convection and subpolar North Atlantic Deep Water export in the SODA assimilation model, Deep-Sea Res. Pt. I, 56, 926–938, 2009.
Stocker, T. F. and Schmittner, A.: Influence of CO_2 emission rates on the stability of the thermohaline circulation, Nature, 388, 862–865, 1997.
Sutton, R. T. and Hodson, D. L. R.: Atlantic Ocean forcing of North American and European summer climate, Science, 309, 115–118, 2005.
Taylor, K. E., Stouffer, R. J., and Meehl, G. A.: An overview of CMIP5 and the experiment design, B. Am. Meteorol. Soc., 93, 485–498, doi:10.1175/BAMS-D-11-00094.1, 2012.
Timmermann, A., An, S. I., Krebs, U. et al.: ENSO suppression due to weakening of the North Atlantic thermohaline circulation, J. Climate, 18, 3122–3139, 2005.
Timmermann, A., Okumura, Y., An, S. I. et al.: The influence of a weakening of the Atlantic meridional overturning circulation on ENSO, J. Climate, 20, 4899–4919, 2007.
Tourpali, K., Schuurmans, C. J. E., van Dorland, R., Steil, B., and Brühl, C.: Stratospheric and tropospheric response to enhanced solar UV radiation: a model study, Geophys. Res. Lett., 30, 1231, doi:10.1029/2002GL016650, 2003.
Vellinga, M. and Wood, R. A.: Global climatic impacts of a collapse of the Atlantic thermohaline circulation, Clim. Change, 54, 251–267, 2002.

CPD
10, 2519–2546, 2014

Wood, R. A., Keen, A. B., Mitchell, J. F. B. et al.: Changing spatial structure of the thermohaline circulation in response to atmospheric CO_2 forcing in a climate model, Nature, 399, 572–575, 1999.

Zhang, R. and Delworth, T. L.: Simulated tropical response to a substantial weakening of the Atlantic thermohaline circulation, J. Climate, 18, 1853–1860, 2005.

Zhang, R., Delworth, T. L., and Held, I. M.: Can the Atlantic Ocean drive the observed multidecadal variability in Northern Hemisphere mean temperature?, Geophys. Res. Lett., 34, L02709, doi:10.1029/2006GL028683, 2007.

CPD
10, 2519–2546, 2014

Table 1. Correlation coefficients of surface density, temperature, and salinity in boxes A and B before and after the abrupt change, respectively. The correlation coefficients in the brackets are for related variables averaged in the oceanic upper layer 300 m. Bold italics indicates the correlation is statistically significant (95 % confidence level).

Region	Cor. Coef.	1900–1917	1917–1950	1900–1950
Box A (50–65° N, 60–45° W)	(rho, *S*)	***0.75 (0.74)***	***0.73 (0.74)***	***0.89 (0.92)***
	(rho, *T*)	***−0.63*** (−0.23)	***−0.43*** (−0.13)	***−0.32*** (0.09)
Box B (50–60° N, 40–30° W)	(rho, *S*)	***0.89 (0.71)***	−0.18 ***(−0.64)***	0.11 ***(−0.43)***
	(rho, *T*)	***−0.83 (−0.86)***	***−0.92 (−0.97)***	***−0.87 (−0.94)***

Note: rho is for density; *S* is for salinity; *T* is for temperature.

CPD
10, 2519–2546, 2014

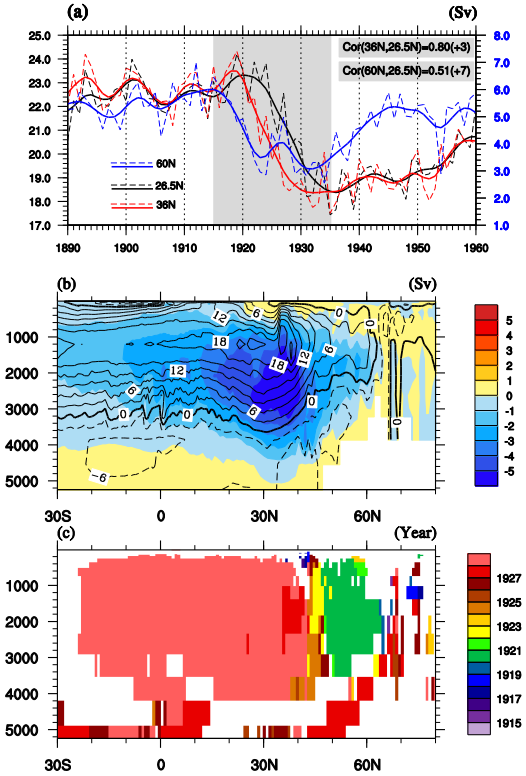

Figure 1. (a) Time series of the maximal Atlantic meridional overturning circulation (AMOC, Sv; 1 Sv = 10^6 m^3 s^{-1}) obtained from 500 m to 3500 m at 26.5° N (black line), 36° N (red line), and 60° N (blue line). Dash and solid lines are for the annual mean and the 7 year running mean values, respectively. The left y-axis is for AMOC at 26.5° N and 36° N, and the right y-axis is for AMOC at 60° N. The shading period is for the abrupt period. **(b)** Annual mean AMOC averaged from 1910 to 1920 (contour) and the differences in AMOC (shading) for 1930–1940 minus 1910–1920. **(c)** The abrupt years of AMOC detected by the moving *t* test technique (MTT).

CPD
10, 2519–2546, 2014

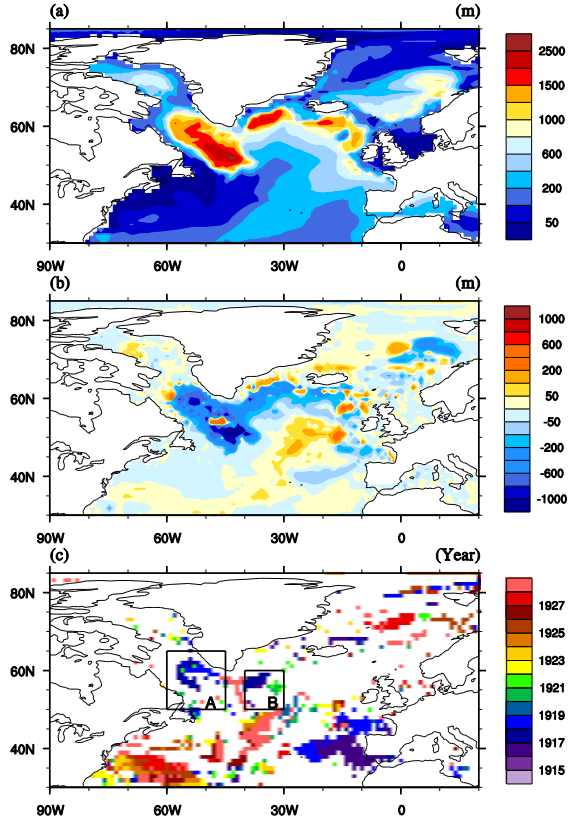

Figure 2. (a) Climatological Mixed-layer depth (MLD, in meters) in the North Atlantic. **(b)** Differences in MLD for 1920–1930 minus 1910–1920. **(c)** The abrupt years of MLD detected by the moving *t* test technique (MTT). Note that the MLD is calculated as the depths in which the potential density is greater than the surface density by approximately 0.03 kg m^{-3}. Black boxes in **(c)** show the key regions for further analysis. Box A is for the region between 60–45° W and 50–65° N. Box B is between 40–30° W and 50–60° N.

CPD
10, 2519–2546, 2014

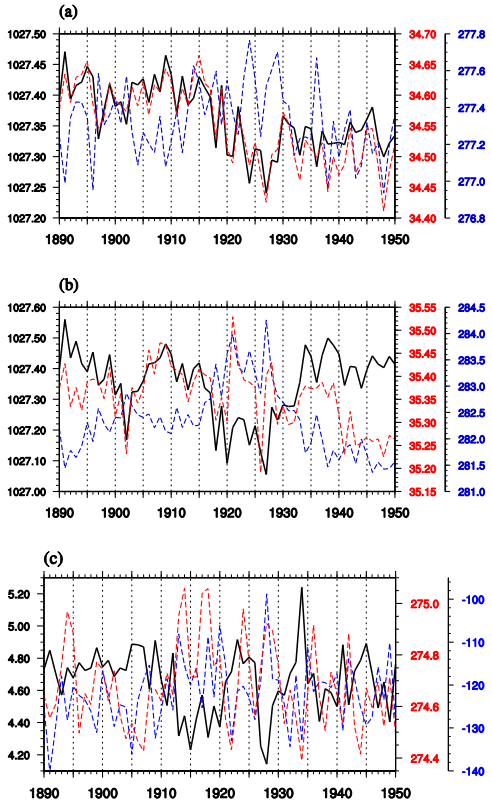

Figure 3. (a) Time series of box A (50–65° N, 60–45° W) averaged potential density (black line), sea surface salinity (red dashed line), and sea surface temperature (SST; blue dashed line). **(b)** Same as **(a)** except for box B at 50–60° N and 40–30° W. **(c)** Time series of regional (60–70° N, 65–50° W) integral sea ice cover averaged from April to September (black line, units: 10^5 km^2), SST (red line, units: K), and surface upwelling shortwave fluxes (blue line; units: W m^{-2}; negative values indicate oceanic heat loss).

CPD
10, 2519–2546, 2014

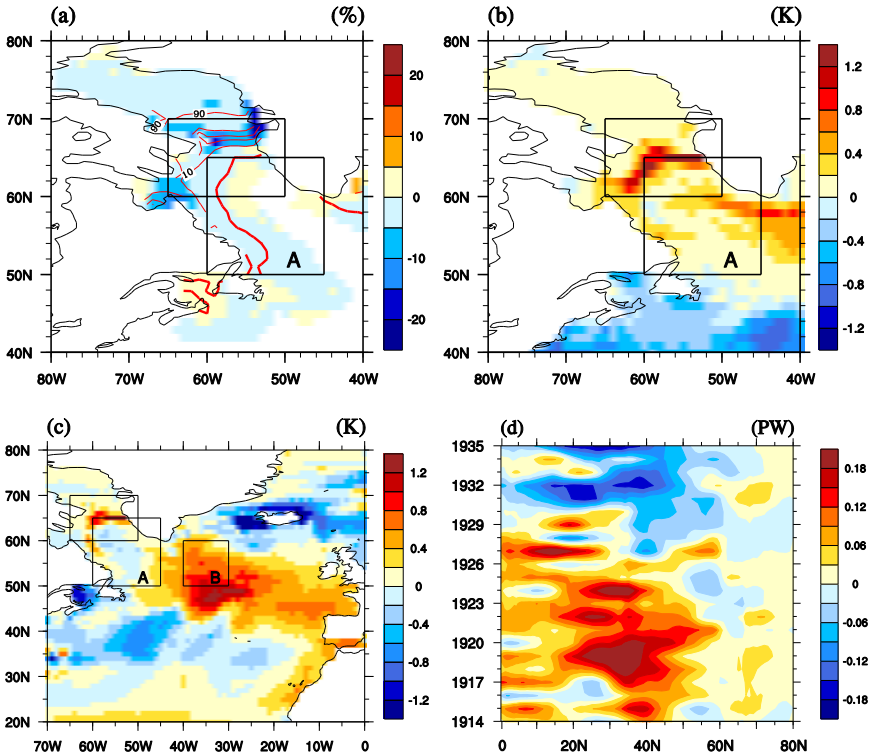

Figure 4. (a) Differences in sea ice concentration (%) from April to September averaged during 1913–1917 minus averaged during 1900–1912. The contour line represents the extent of sea ice averaged from 1900 to 1912. **(b)** Same as **(a)** except for sea surface temperature (SST, units: K). **(c)** Same as **(b)** except for SST differences (1917–1918 minus 1910–1916). **(d)** Latitude–Time diagrams of northward ocean heat transport (units: PW; $1\,\mathrm{PW} = 10^{15}\,\mathrm{W}$). Anomalies are relative to 1860–1900 in the North Atlantic. Box A and B are same as those in Fig. 2c. The box in northwest location is for the region where the sea ice melting is the most significant.

CPD
10, 2519–2546, 2014

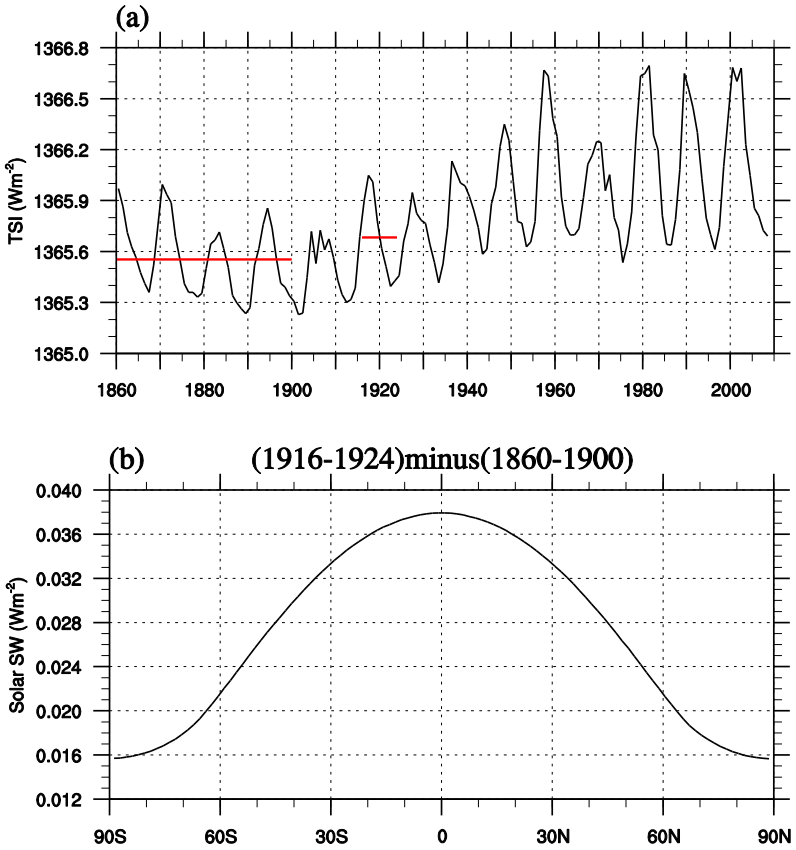

Figure 5. (a) Time series of annual mean total solar irradiance (TSI, units: W m^{-2}). The two red lines are for the mean values of 1860–1900 and 1916–1924 with the value of 1365.55 W m^{-2} and 1365.68 W m^{-2}, respectively. **(b)** Differences in zonal mean incoming shortwave radiation at the top-of-atmosphere (units: W m^{-2}) averaged from 1916 to 1924 and from 1860 to 1900.

CPD
10, 2519–2546, 2014

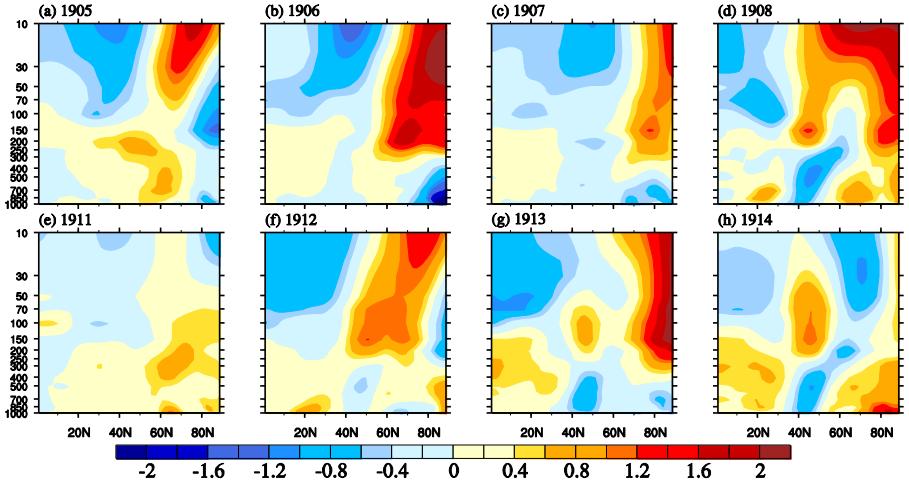

Figure 6. Meridional–vertical sections of the zonal mean air temperature anomalies (averaged from 70–0° W, units: K) relative to 1860–1900 in **(a)** 1905, **(b)** 1906, **(c)** 1907, **(d)** 1908, **(e)** 1911, **(f)** 1912, **(g)** 1913, **(h)** 1914.

CPD
10, 2519–2546, 2014

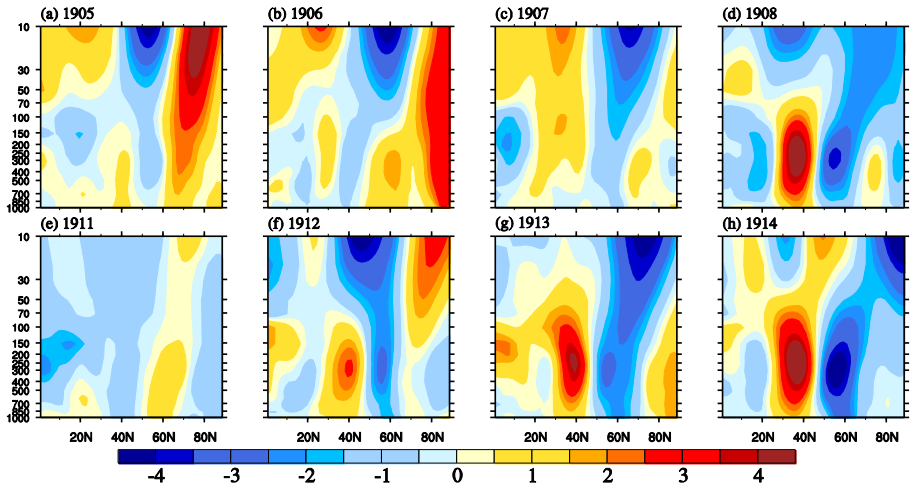

Figure 7. Meridional–vertical sections of the zonal mean zonal wind anomalies (averaged from 70–0° W, units: m s^{-1}) relative to 1860–1900 in **(a)** 1905, **(b)** 1906, **(c)** 1907, **(d)** 1908, **(e)** 1911, **(f)** 1912, **(g)** 1913, **(h)** 1914.

CPD
10, 2519–2546, 2014

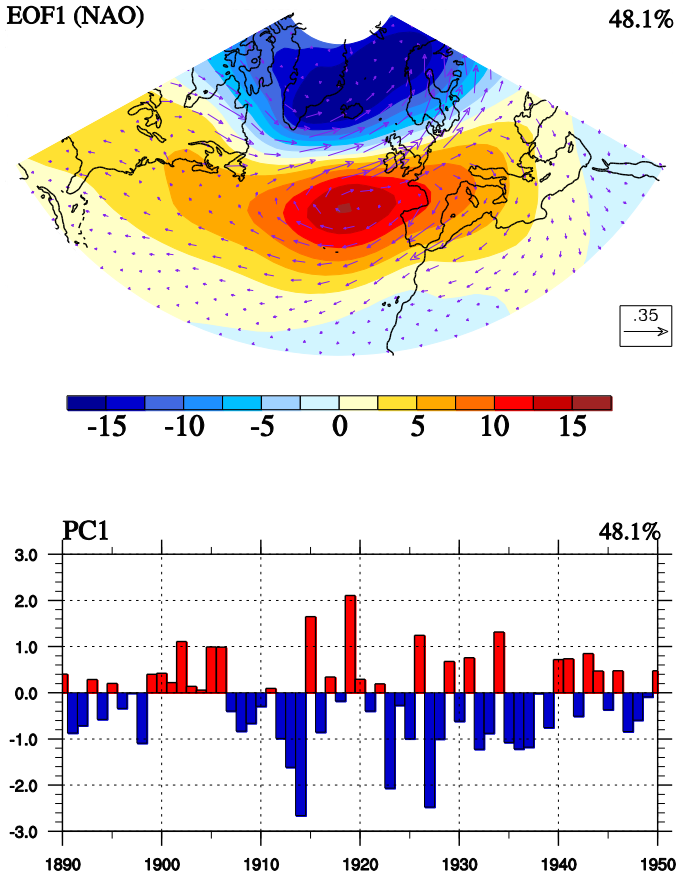

Figure 8. The leading multivariate EOF pattern (upper) and corresponding PC of annual mean sea level pressure (shaded) and wind stress (vectors) over the North Atlantic region (90° W–40° E). The percentage of variance explained by the first EOF is shown in the top right corner of each plot.

CPD
10, 2519–2546, 2014